Self-assembly-Directed Cancer Cell Membrane Insertion of Synthetic Analogues for Permeability Alteration

Enming Du,[†] *Xunwu Hu,*[†] *Guanying Li,*[†] *Shijin Zhang,*[†] *Dingze Mang,*[†] *Sona Roy,*[†] *Toshio Sasaki,*[‡] *and Ye Zhang**[†]

[†]Bioinspired Soft Matter Unit, [‡]Imaging Section, Okinawa Institute of Science and Technology Graduate University, 1919-1 Tancha, Onna-son, Okinawa, 904-0495, Japan

Self-assembly, Cancer cell, Membrane Insertion, rigid molecule, permeability alteration

ABSTRACT

Inspired by the metamorphosis of pore-forming toxins (PFTs) from soluble inactive monomers to cytolytic transmembrane assemblies, we developed self-assembly-directed membrane insertion of synthetic analogues for permeability alteration. An expanded π-conjugation based molecular precursor with extremely high rigidity, long hydrophobic length that comparable to the hydrophobic width of plasma membrane, is synthesized for membrane inserted self-assembly. Guided by the cancer biomarker expression in vitro, the soluble precursors transform into hydrophobic monomers for self-assembly structure inserting into the fluid phase of membrane

exclusively. Membrane insertion of rigid synthetic analogue destroys the selective permeability of the plasma membrane gradually. It eventually leads to cancer cell death, including drug resistant cancer cells.

INTRODUCTION

Selective permeability is one of the key features of cell membrane to maintain its functionality as active barrier between life and death. Altering the membrane permeability not just leads to cell death, but also potentially leads to subtle manipulation of cellular functions. The mechanistic insights of membrane targeting proteins enable the development of novel therapeutic strategies. Unfortunately, the application of membrane modification and manipulation as part of cancer therapy is lagging.[1-2]

As a major class of pore-forming proteins, PFTs have been well known for altering the plasma membrane permeability of their target cells.[3] The targeted surface binding leads to a drastic increase in a local concentration triggering the oligomerization of PFTs. Upon the exposure of hydrophobic surfaces in the transition process, PFTs insert into membrane leading to cell death. These mechanistic insights inspired us to design a potential cancer therapeutic strategy using molecular self-assembly facilitated membrane insertion of synthetic analogues on cancer cells. As shown in Figure 1, non-toxic water-soluble molecular precursors are constructed to mimic the inactive hydrophilic PFT monomers distributed in extracellular fluid. Under tumor microenvironment, the alkaline phosphatases (ALPs) that over expressed by cancerous cells dephosphorylate the precursors into hydrophobic building blocks upon cell membrane triggering self-assembly into rigid aggregates.[4-8] The hydrophobic surface of the aggregate facilitates its insertion into the hydrocarbon core of membrane constructing nanoarchitectonics among the

phospholipid bilayer.[9-11] The porosity binding effect with molecules of the inserted synthetic analogues lead to membrane permeability alteration by blocking the transportation of molecules. Severe permeability alteration eventually leads to cancer cell death.

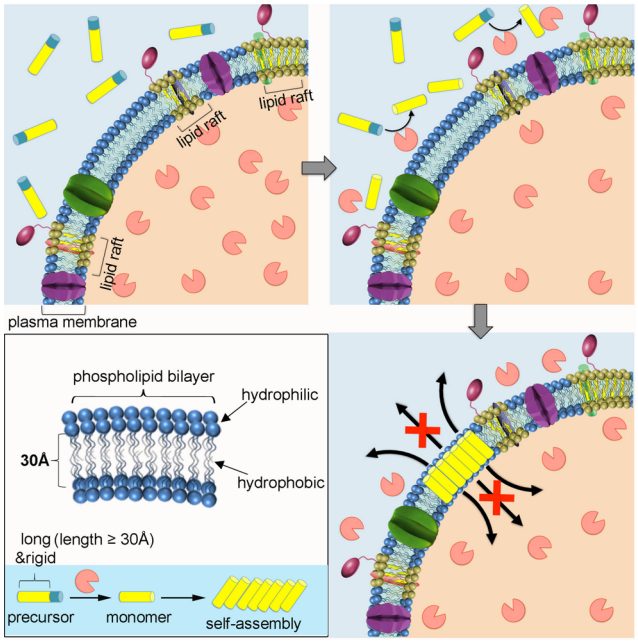

Figure 1. Schematic illustration of self-assembly directed membrane insertion of long and rigid synthetic analogue causing permeability alteration.

Regarding the complexity and dynamic features of membrane structure, the live cell membrane insertion of synthetic analogues, without the help of external force, is difficult and challenging. Except single molecular synthetic peptides derived from natural proteins or peptides,[12] live cell membrane insertion of sub-micron synthetic structures was rarely reported.[13] Computational simulations indicate that besides intrinsic rigidity of the synthetic analogue, a proper length of the purely hydrophobic portion match to the hydrophobic core of the membrane to maximize the interactions[13] is also critical to the successful insertion.[14] Therefore, we select the hydrophobic domain of 'muscle molecule',[15-16] the expanded π-conjugation system with extremely high rigidity,

long linear length, for the construction of desired molecular precursor leading to self-assembly-guided membrane insertion.

EXPERIMENTAL SECTION

Materials and Instruments. Ammonium acetate was purchased from Nacalai Tesque, INC. and purified by sublimation before usage. Other chemical reagents were purchased from Sigma, Nacalai and Wako and used without further purification. Mass spectra were recorded using a Thermo LTQ-ETD mass spectrometer (ESI) and high resolution mass spectra were measured with a Thermo LTQ-Orbitrap Classic mass spectrometer (ESI). ^{1}H, ^{13}C and ^{31}P NMR spectra were recorded on a Bruker Ascend 400 (400, 100 and 162 MHz, respectively) spectrometer. Time-dependent ^{31}P NMR for dephosphorylation process was recorded on a JEOL 600 MHz NMR (243 MHz). TEM micrographs were obtained on a JEM-1230R Transmission Electron Microscope. SEM micrographs were measured on a FEI Quanta 250 FEG Scanning Electron Microscope. Confocal images were obtained on a Zeiss LSM780 Confocal Microscope. The fluorescence intensity of PI was detected using imaging flow cytometer (ImageStream X Mark, Germany). LDH release was determined using a Tecan Infinite M1000 PRO microplate reader.

Synthesis. Synthetic procedures and characterizations of surface ligands applied in this study are described in Supporting Information.

TEM imaging. Aliquots (10 μL) of sample solution were added into a glow discharge copper grid (400 mesh) coated with thin carbon film and incubated for 30 s at room temperature. After removing excess solution, the grid was washed with deionized water three times and then stained with 2.0% (w/v) uranyl acetate (UA) by exposing the grid in three drops of UA solution for 30 s.

TEM images were captured at high vacuum on transmission electron microscope JEM-1230R (JEOL, Japan).

Molecular dynamics simulations and polymorph prediction. Molecular mechanics calculations were performed using Materials Studio. As the crystal structure prediction method uses a rigid body approximation in the initial search for crystal packing alternatives, it is necessary to perform an analysis to determine low energy geometry to be used as input for the packing calculations. The molecules were drawn and geometrical energy minimization scans were performed using Forcite module of Materials Studio. The optimized low energy conformations were used as the starting points for crystal structure prediction using the Materials Studio Polymorph Predictor (PP).

Cell viability assay. Cells in exponential growth phase were seeded in a 96 well plate at a concentration of 7×10^3 cells/well for HeLa, A375, and 1×10^4 cells/well for HS5, OVCAR3, cell lines. The cells were allowed to attach to the wells for 12 h at 37ºC, 5% CO_2. The culture medium was removed followed by addition of 100 μL culture medium containing different concentrations (0.1, 1, 10, 100 and 200 μM) of compound **2** (immediately diluted from 10 mM stock solution in PBS buffer). After the desired time of exposure, 10 μL MTT solution (5 mg/mL) was added to each well and incubated at 37°C for another 4 h, and then 100 μL of SDS solution (10% in Milli-Q water) was added to stop the reduction reaction and dissolve the purple formazan. The absorbance of each well at 570 nm was measured by a Tecan microplate reader. All experiments were conducted triplicate. The results were calculated as means, which are expressed as cell viability (%).

Live Cell imaging. Molecular probes were purchased from Life Technologies (Thermo Fisher Scientific, USA). Cells in exponential growth phase were seeded into a glass bottomed culture

dish at 2×10^5 cells per dish. The cells were allowed for attachment for 24 h at 37 °C under 5% CO_2. Culture medium was removed and fresh medium containing different concentrations of compounds was added. After incubation for desired time, cells were washed with live cell imaging solution for three times, and further stained with commercial cell labels. Cells were then washed two times with fresh live-cell imaging solution and visualized by laser confocal microscopy (LSM 780, Carl Zeiss) immediately (λ_{ex}: 405 nm for compound **2**, 488 nm for Lysotracker Green DND-26, 561 nm for Actinred 555 and Alexa Fluor 555, 633 nm for CellMask deep red; λ_{em}: 420-480 nm for compound **2**, 508-570 nm for Lysotracker Green DND-26, 580-720 nm for Actinred 555, 570-606 nm for Alexa Fluor 555, 650-750 nm for CellMask deep red).

SEM imaging. After taking confocal images, the samples were washed with PBS and then the cells were cross-linked with 2.5% glutaraldehyde in 0.1 M cacodylate buffer for 10 min. The samples were washed with 0.1 M cacodylate buffer for 5 min (×3) and then further fixed with 1% osmium tetroxide in 0.1 M cacodylate buffer for 30 min, followed by washing with water for 5 min (×3) and then progressive dehydration in a graded series of ethanols (70%, 80%, 90%, 95% and twice in 100%, 3 minutes at each concentration). The cells were rinsed with *t*-butanol for 3 min (×3) and then dried by freeze-dryer overnight. SEM images of the dried samples were captured before platinum coating.

LDH release. LDH release activity was measured by pierce LDH cytotoxicity assay kit (Thermo Scientific) according to the manufacturers' instructions. HeLa, A375 and OVCAR3 cells were seeded at 1.5×10^4 cells/well in 100 μL of medium in a 96 well plate, respectively. After incubation with compound **2** (10, 50, 100 μM) for 12 h, the release of LDH in the supernatant was measured with a microplate reader at 490 nm. Cells treated with 10 μL of water

(12 h) or Lysis buffer (10X, 45 min) was used as negative and positive controls, respectively. All experiments were carried out in triplicates. LDH activity was calculated as follows:

$$\text{LDH release (\%)} = \frac{\text{Compound treated activity} - \text{Negative activity}}{\text{Positive activity} - \text{Negative activity}} \times 100$$

RESULTS AND DISCUSSION

Molecular design and synthesis.1,10-phenanthroline analogous containing two bidentates were reported as optimal ligands in the preparation of multinuclear cyclic pseudorotaxanes as ′muscle molecules′ through metal(I)-mediated assembly because of their long linear length and highly rigidity. By replacing the polyethylene glycol macrocycle with two carboxyl groups, we were able to introduce enzyme responsive amino acids obtaining the target molecule **2** (Scheme 1A). The synthesis commences with 2,9-dibromo-1,10-phenanthroline and 3,8-dibromo-1,10-phenanthroline both prepared from 1,10-phenanthroline through different paths (Scheme S1 and S2). Following Sauvage's method, we were able to apply 2,9-dibromo-1,10-phenanthroline and methyl 4-(5,5-dimethyl-1,3,2-dioxaborinan-2-yl)benzoate for Suzuki-coupling obtaining the dione building block in elevated yield (84%). The linear aldehyde building block was prepared in 5 steps from 3,8-dibromo-1,10-phenanthroline. A condensation of both building blocks at the presence of ammonium acetate in a sealed tube at 105°C for 24 h constructed an oxazole ring as rigid spacer leading to molecule **1** identified by high-resolution mass spectroscopy (HRMS). Two carboxyl groups of the rigid molecule **1** were activated with diisopropylcarbodiimide (DIC) and *N*-hydroxysuccinimide (NHS), following the conjugation with two *o*-phospho-L-tyrosine (Yp) forming the soluble precursor **2**. Upon the expression of alkaline phosphatase (ALP), the precursor **2** transforms into **3**, the hydrophobic monomer ready for self-assembly.

The geometrical energy minimized structures of 2 and 3 (Scheme 1B) indicate both molecules adopt Y-shape with linear length of hydrophobic domain beyond 30 Å,[1] longer than the thickness of the hydrophobic core of cell membrane. The hydrophobic domains of both molecules remain static without deformation during ALP induced dephosphorylation due to the extreme rigidity, which may lead to efficient membrane insertion.

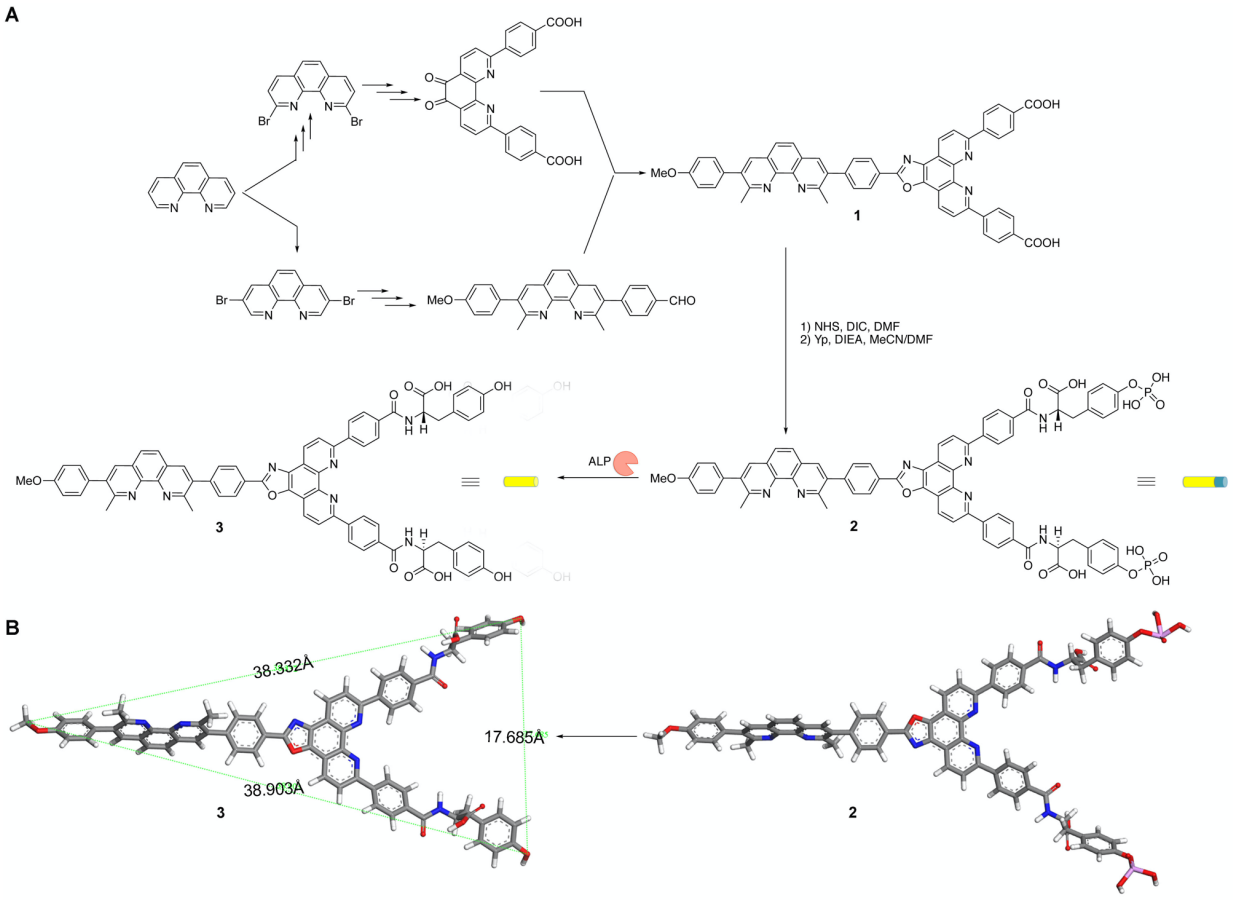

Scheme 1. (A) The synthetic path of precursor 2, and the enzyme triggered transformation of 2 into monomer of self-assembly 3. (B) The stick models of geometrical energy minimized structures of 2 and 3.

ALP induced molecular self-assembly. The ALP instructed transformation of **2** into **3** was monitored by ^{31}P NMR (Figure 2A).[17] The time-lapse spectra indicated that after 90 min incubation with ALP (Figure S1B), a complete conversion of **2** to **3** is reached. Time-lapse emission spectroscopies (Figure 2B and S1) indicate the decrease of emission intensity during the first 60-min incubation induced by self-quenching. After that, the intensity gradually becomes stable. The two-stage migration of maximum emission peak, red shift until 60 min and blue shift afterwards, suggests a dynamic adjustment of molecular packing following the molecular transformation from **2** to **3**. Regarding the rigidity of the molecule, the intermolecular π–π stacking is suggested as the main driving force for self-assembly resulting in the overall red shift (from 457nm to 475 nm) of emission spectra. Optical images taken at the end-point of the transformation exhibit clear solutions with neither precipitation nor gel-formation observed. Under the UV light, the solution emits light blue fluorescence (Figure 2C and S2). The transmission electron microscopy (TEM) (Figure 2D and S2) confirms the self-assembly of **3** into irregular nanoscale aggregates distributed in PBS buffer. The Polymorph Predictor module[18] predicts molecular self-assembly is driven by strong intermolecular π-π stacking (Figure 2E and Figure S3) forming close packed nanostructure with hydrophobic surface, which is consistent to the emission spectra variations.

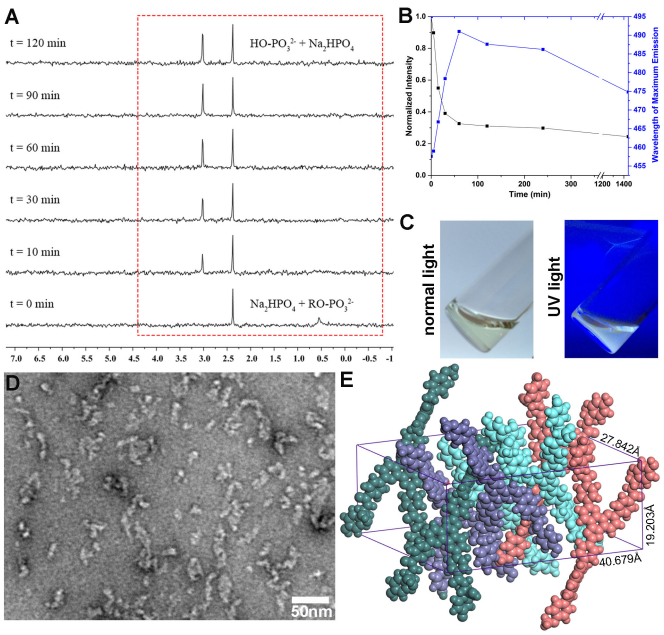

Figure 2. (A) Time-lapse ^{31}P NMR spectroscopies of **2** (400 μM) in Tris-HCl D_2O buffer (50mM, pH = 8.5) reacting with ALP (1 U/mL). Na_2HPO_4 (6mM) is used as internal standard. (B) Time-lapse normalized maximum emission intensity and wavelength of **2** (100 μM) in PBS buffer reacted with ALP (1 U/mL). Optical images under the normal light and UV light (365 nm) (C) and TEM image (D) of end-point of **2** (100 μM) reacted with ALP (1U/mL) in PBS buffer. (E) The predicted molecular stacking of **3** in CPK model correlated to the self-assemblies in TEM image.

Membrane insertion induced toxicity *in vitro*. Three cancer cell lines, the cervical cancer cell (HeLa), the skin malignant melanoma cell (A375), the drug resistant ovarian cancer cell (OVCAR-3), and stromal cell line HS-5 cell with ALP isozymes in different expression patterns cultured in different concentrations of exogenous ALP (the ALP expression profiles are summarized in Table S1), are applied in cytotoxicity tests of **2** (Figure 3A). With no toxicity on HS-5 cells, cancerous cell targeted cytotoxicity of **2** is revealed. Cancerous cell viability profiles also suggested concentration dependent/cell type dependent toxicity of **2**. **2** started showing

toxicity on HeLa cell beyond 10 μM. But it started showing toxicity on both A375 cell and OVCAR3 cell beyond 100 μM. At 200 μM, **2** had similar toxicity on both HeLa and A375 cells. And it killed 40% of the OVCAR3 cells after 3-day incubation.

Live cell imaging by confocal microscopy exhibits toxicity correlated selective subcellular targeting. Towards cancerous cells, under compatible condition ([**2**] =10 μM), we observe blue fluorescence distributed mainly in lysosomes (Figure S4A). Accompanied with cytotoxicity, self-assemblies start accumulating on cell membranes with stochastic distribution. Following the rising of toxicity, the population of targeted cell by self-assemblies rises (Figure S4B and S4C). Comparing to normal cell (HS-5)'s lysosome targeted accumulation of self-assemblies (Figure S5), precursor **2** selectively target cancerous cell membranes inducing toxicity. Fluorescent imaging along the z-axis (Figure 3B, 3C 3D and S6) reveals cancerous cell membrane insertion of self-assemblies. The fluorescent intensity profile along the cell membrane exhibiting enhancement of self-assemblies' fluorescent intensity (blue) accompanied with decline of cell membrane's fluorescent intensity (red) vice versa, confirms the membrane insertion of self-assemblies on three types of cancerous cells. Under the same incubation condition, the membrane insertion rate in order from the highest to the lowest is HeLa cell, A375 cell and OVCAR-3 cell, consistent to the cytotoxicity profile of **2** towards these cancer cells. SEM images indicated microscale synthetic analogues inserting on membrane close to the cell margin of all three types of cancerous cells (Figure S7). By increasing the incubation concentration of **2**, expansion of assembled analogues on membrane is observed (Figure S4B and S4C). Scientists predicted the phospholipids exaction from membrane to inserted analogue due to the van der Waals and hydrophobic interactions during the late stage of insertion.[19] We observed the same

phenomenon in the experiment that the membrane shifted toward self-assembled analogues (Figure S8).

ALP guided membrane insertion *in vitro*. The non-selective membrane insertion on all three types of cancer cells with (HeLa) and without (A375 and OVCAR3) placental alkaline phosphatase (PLAP) expression suggests that overexpression of PLAP that locate on the membrane is not critical to self-assembly-facilitated membrane insertion here. After treatment of PLAP inhibitor L-phenylalanine, HeLa cells showed unaffected membrane insertion of assembled analogues (Figure S9). HeLa cell membrane insertions show no overlap with PLAP (Figure 4A) suggest no physical binding interactions between the PLAP and self-assemblies, which is different from PLAP guided self-assembly on cancer cell membrane showing co-localizations.[4-5, 7-8, 20-21] By removing the exogenous ALP in the culture medium, higher membrane insertion efficiency is observed (Figure S10). These experimental results indicate that the membrane insertion of self-assembled analogues is a consequence of collective influence of cancer cell released ALP, and the exogenous ALP.

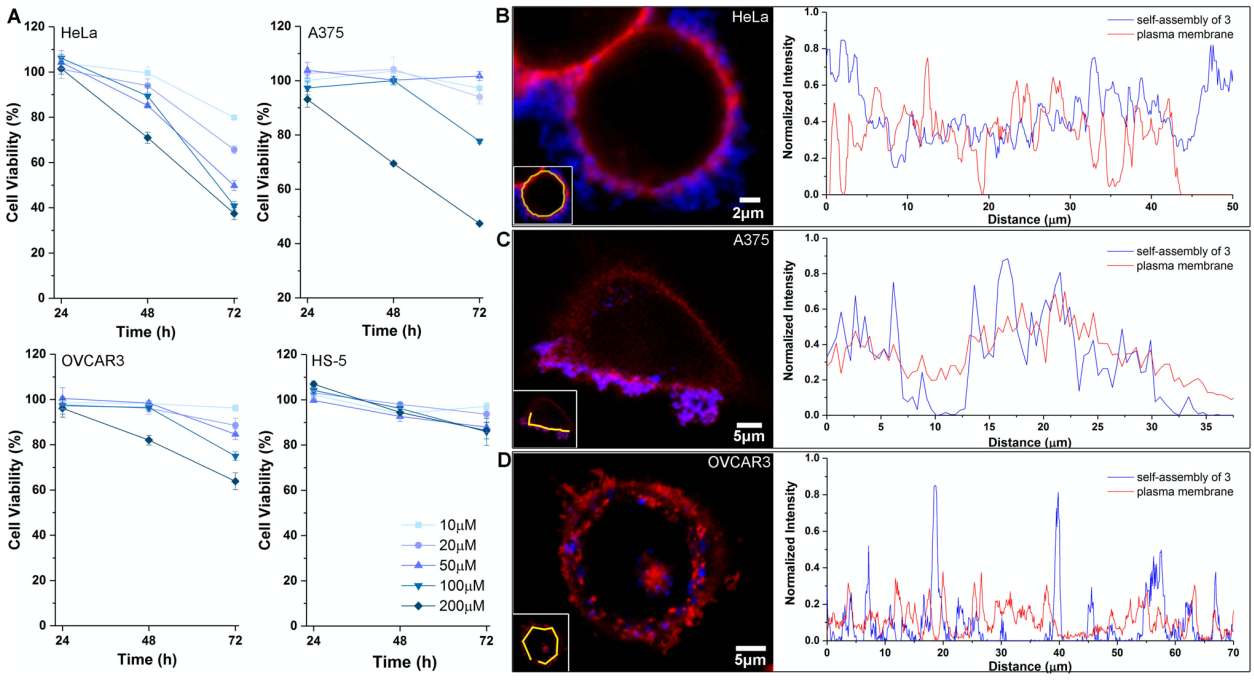

Figure 3. (A) Cell viabilities of HeLa, A375, OVCAR3 and HS-5 cells treated with precursor 2 at various concentrations. Confocal image (one section along the z-axis) and fluorescent intensity profile of HeLa (B), A375 (C) and OVCAR3 (D) cells treated with 2 (100 μM) for 24 h and stained with CellMask-deep red. The inlet picture in confocal image indicates the fluorescent intensity profile area by yellow line. In both confocal images and intensity profiles, blue represents self-assemblies and red represents plasma membrane.

Selective membrane insertion in fluid phase. Heterogeneity is essence to membrane structure. Membrane lipids with varying lengths of hydrophobic portion adopt various fluid and solid phases through relatively loose packing with narrower hydrophobic core or tight packing with hydrophobic region in longer length, respectively.[1] In model bilayer with coexisted fluid and solid phases, functional peptide or protein show clear preference for a particular phase. Therefore, besides physical properties alteration, membrane insertion into fluid phase or solid phase will induce remarkably different cellular biochemical transductions. To detect the specificity of membrane insertion, we apply lipid raft marker to label the solid phase of HeLa cell membrane after treatment with precursor **2**. Imaging along the z-axis (Figure 4B and Figure S11) indicates that the self-assemblies selectively insert into fluid phase of membrane avoiding solid phase, the lipid rafts,[22] which is different from the PLAP guided self-assembly reported previously.[4, 23] This is confirmed by fluorescence intensity profile of the cell margin that exhibits enhancement of fluorescent intensity of self-assemblies (blue) accompanied with decline of fluorescent intensity of lipid rafts (green), vice versa (Figure 4B).

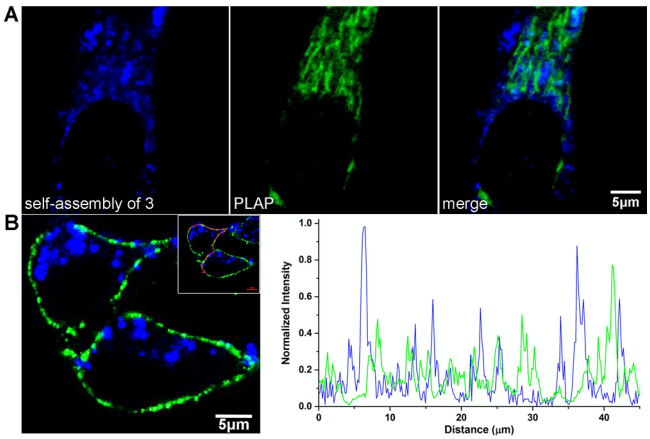

Figure 4. (A) Confocal images of HeLa cell treated with precursor **2** for 24 hours with PLAP labelling. (B) Confocal image (left) of HeLa cell treated with **2** (100 μM) for 24 h and stained with Lipid Raft Labeling (green), and fluorescent intensity profile (right) of self-assemblies (blue) and lipid rafts (green) along the cell margin indicated by red line in inlet confocal image. Self-assemblies are represented in blue. Membrane inserted matrix between rafts are indicated by light blue arrows.

Membrane insertion induced permeability alteration. To study the membrane permeability alteration, the cellular uptake or release of small organic molecule, peptide and protein after membrane insertion were characterized. We selected 5-chloromethylfluorescein diacetate (CellTracker Green), fluorescently labeled phalloidin (ActinRed) and lactate dehydrogenase (LDH), representing the three types of molecules respectively.

We applied patch pipette tips tightly contacting the plasma membrane of cells with and without membrane insertion of self-assembly of **3** as shown in Figure 5A. By releasing the fluorescent CellTracker Green, we recorded the time-lapse intracellular fluorescent intensity as summarized in Figure 5A. Clearly, the membrane insertion results into inhibition of intracellular uptake of small organic molecules. ActinRed, as a live cell membrane impermeable bi-cyclic peptide, is applied in HeLa cell culture after cell incubation with **2** without fixing and permeabilizing the

cell. The confocal images (Figure 5B) show no intracellular actin stain after membrane insertion suggesting not only the peptide can't pass through the inserted synthetic analogues, but also the un-inserted part of cell membrane is intact. The co-localization of ActinRed with membrane inserted self-assembled analogues indicates the binding interactions between them. A negligible increase of LDH release was also observed in all the cancerous cells incubated with precursor **2** at increasing concentrations for 12 h (Figure 5C).

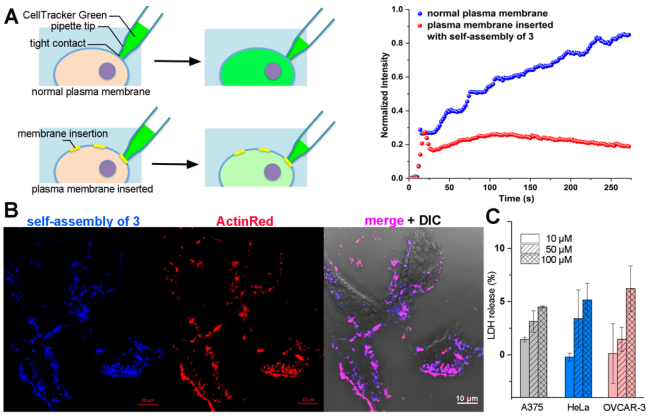

Figure 5. (A) Schematic illustration of protocol applied for cell uptake of CellTracker Green before and after membrane insertion (left) and the time-lapse intracellular fluorescent intensity profile (right) obtained by following the protocol. (B) Confocal images of HeLa cells treated with **2** (100 μM) for 24 h and stained with ActinRed without fixing and permeabilizing the cell. (C) Extracellular release of LDH in different cancerous cell lines after incubation with increasing concentrations of precursor **2** for 12 h.

The experiment results indicate that the membrane insertion of self-assembled analogues alters the cell membrane permeability by blocking the intracellular uptake without general membrane disturbance. Eventually, the expansion of membrane insertion of synthetic analogues totally blocks the cell metabolism and leads to cell death.

CONCLUSIONS

The application of extremely rigid molecule in tumour biomarker induced molecular self-assembly successfully implements the cancer cell membrane insertion of synthetic micro-scale analogues *in vitro*. Interestingly, the self-assembled system only inserts into the fluid phase of cancerous cell membrane altering the membrane permeability. The selectivity and membrane insertion efficiency on several cancer cell lines demonstrate the potential of the design as anticancer strategy. On the other hand, the relatively mild cytotoxicity on certain cancer cell lines indicates the potential of subtle manipulation of cellular functions. The main challenges ahead are to comprehensively characterize the kinetics of this process and to modify the molecular design for cancer therapeutics. Undoubtedly, the study of cell response to membrane insertion of self-assemblies at molecular level will also facilitate the mechanism exploration of membrane repair and danger sensing.

ASSOCIATED CONTENT

Supporting Information. Synthesis and characterization of molecules, cell viability assay, live cell imaging, membrane permeability characterization assay are included in supporting information.

AUTHOR INFORMATION

Corresponding Author

*E-mail: ye.zhang@oist.jp.

ACKNOWLEDGMENT

This work was supported by Okinawa Institute of Science and Technology Graduate University, and Takeda Science Foundation.

REFERENCES

(1) van Meer, G.; Voelker, D. R.; Feigenson, G. W., Membrane lipids: where they are and how they behave. *Nat Rev Mol Cell Bio* **2008,** *9*, 112-124.
(2) Zalba, S.; ten Hagen, T. L. M., Cell membrane modulation as adjuvant in cancer therapy. *Cancer Treat Rev* **2017,** *52*, 48-57.
(3) Dal Peraro, M.; van der Goot, F. G., Pore-forming toxins: ancient, but never really out of fashion. *Nat Rev Microbiol* **2016,** *14*, 77-92.
(4) Li, G.; Sasaki, T.; Asahina, S.; Roy, M. C.; Mochizuki, T.; Koizumi, K.; Zhang, Y., Patching of Lipid Rafts by Molecular Self-Assembled Nanofibrils Suppresses Cancer Cell Migration. *Chem* **2017,** *2*, 283-298.
(5) Pires, R. A.; Abul-Haija, Y. M.; Costa, D. S.; Novoa-Carballal, R.; Reis, R. L.; Ulijn, R. V.; Pashkuleva, I., Controlling Cancer Cell Fate Using Localized Biocatalytic Self-Assembly of an Aromatic Carbohydrate Amphiphile. *J Am Chem Soc* **2015,** *137*, 576-579.
(6) Wang, H. M.; Feng, Z. Q. Q.; Wu, D. D.; Fritzsching, K. J.; Rigney, M.; Zhou, J.; Jiang, Y. J.; Schmidt-Rohr, K.; Xu, B., Enzyme-Regulated Supramolecular Assemblies of Cholesterol Conjugates against Drug-Resistant Ovarian Cancer Cells. *J Am Chem Soc* **2016,** *138*, 10758-10761.
(7) Zhou, J.; Du, X.; Berciu, C.; He, H.; Shi, J.; Nicastro, D.; Xu, B., Enzyme-Instructed Self-Assembly for Spatiotemporal Profiling of the Activities of Alkaline Phosphatases on Live Cells. *Chem* **2016,** *1* (2), 246-263.
(8) Zhou, J.; Du, X. W.; Yamagata, N.; Xu, B., Enzyme-Instructed Self-Assembly of Small D-Peptides as a Multiple-Step Process for Selectively Killing Cancer Cells. *J Am Chem Soc* **2016,** *138* (11), 3813-3823.
(9) Cymer, F.; von Heijne, G.; White, S. H., Mechanisms of Integral Membrane Protein Insertion and Folding. *J Mol Biol* **2015,** *427*, 999-1022.
(10) Ariga, K.; Mori, T.; Li, J., Langmuir Nanoarchitectonics from Basic to Frontier. *Langmuir* **2018**.
(11) Komiyama, M.; Yoshimoto, K.; Sisido, M.; Ariga, K., Chemistry Can Make Strict and Fuzzy Controls for Bio-Systems: DNA Nanoarchitectonics and Cell-Macromolecular Nanoarchitectonics. *B Chem Soc Jpn* **2017,** *90*, 967-1004.
(12) Boohaker, R. J.; Lee, M. W.; Vishnubhotla, P.; Perez, J. M.; Khaled, A. R., The Use of Therapeutic Peptides to Target and to Kill Cancer Cells. *Curr Med Chem* **2012,** *19* (22), 3794-3804.
(13) Geng, J.; Kim, K.; Zhang, J. F.; Escalada, A.; Tunuguntla, R.; Comolli, L. R.; Allen, F. I.; Shnyrova, A. V.; Cho, K. R.; Munoz, D.; Wang, Y. M.; Grigoropoulos, C. P.; Ajo-Franklin, C. M.; Frolov, V. A.; Noy, A., Stochastic transport through carbon nanotubes in lipid bilayers and live cell membranes. *Nature* **2014,** *514*, 612-615.
(14) Lopez, C. F.; Nielsen, S. O.; Moore, P. B.; Klein, M. L., Understanding nature's design for a nanosyringe. *P Natl Acad Sci USA* **2004,** *101*, 4431-4434.
(15) Kraus, T.; Budesinsky, M.; Cvacka, J.; Sauvage, J. P., Copper(I)-directed formation of a cyclic pseudorotaxane tetramer and its trimeric homologue. *Angew. Chem. Int. Ed.* **2006,** *45*, 258-61.
(16) Voignier, J.; Frey, J.; Kraus, T.; Budesinsky, M.; Cvacka, J.; Heitz, V.; Sauvage, J. P., Transition-metal-complexed cyclic [3]- and [4]pseudorotaxanes containing rigid ring-and-filament conjugates: synthesis and solution studies. *Chem. Eur. J.* **2011,** *17*, 5404-14.
(17) Shi, J. F.; Yuan, D.; Haburcak, R.; Zhang, Q.; Zhao, C.; Zhang, X. X.; Xu, B., Enzymatic Dissolution of Biocomposite Solids Consisting of Phosphopeptides to Form Supramolecular Hydrogels. *Chem-Eur J* **2015,** *21*, 18047-18051.
(18) Li, H. Q.; Bahuleyan, B. K.; Johnson, R. P.; Shchipunov, Y. A.; Suh, H.; Ha, C. S.; Kim, I., Morphology-tunable architectures constructed by supramolecular assemblies of alpha-diimine compound: fabrication and application as multifunctional host systems. *J Mater Chem* **2011,** *21*, 17938-17945.
(19) Gu, Z. L.; Yang, Z. X.; Luan, B. Q.; Zhou, X. F.; Hong, L. B.; Zhou, H.; Luo, J. D.; Zhou, R. H., Membrane Insertion and Phospholipids Extraction by Graphyne Nanosheets. *J Phys Chem C* **2017,** *121*, 2444-2450.
(20) Kuang, Y.; Shi, J. F.; Li, J.; Yuan, D.; Alberti, K. A.; Xu, Q. B.; Xu, B., Pericellular Hydrogel/Nanonets Inhibit Cancer Cells. *Angew Chem Int Edit* **2014,** *53*, 8104-8107.
(21) Feng, Z. Q. Q.; Wang, H. M.; Zhou, R.; Li, J.; Xu, B., Enzyme-Instructed Assembly and Disassembly Processes for Targeting Downregulation in Cancer Cells. *J Am Chem Soc* **2017,** *139*, 3950-3953.
(22) Rajendran, L.; Simons, K., Lipid rafts and membrane dynamics. *J Cell Sci* **2005,** *118*, 1099-1102.
(23) Wang, H. M.; Feng, Z. Q. Q.; Del Signore, S. J.; Rodal, A. A.; Xu, B., Active Probes for Imaging Membrane Dynamics of Live Cells with High Spatial and Temporal Resolution over Extended Time Scales and Areas. *J Am Chem Soc* **2018,** *140*, 3505-3509.

TOC

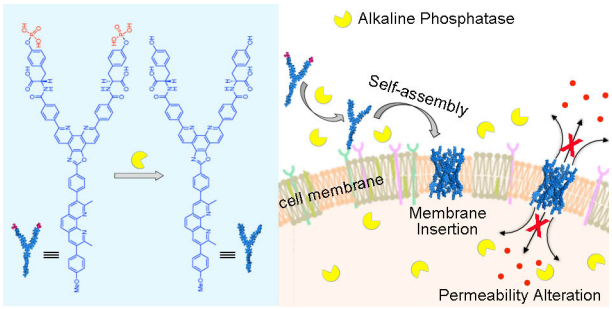
Alkaline Phosphatase
Self-assembly
cell membrane
Membrane
Insertion
Permeability Alteration